

Eumelanin Buildup on the Nanoscale: Aggregate Growth/Assembly and Visible Absorption Development in Biomimetic 5,6-Dihydroxyindole Polymerization.

Marianna Arzillo,[†] Gaetano Mangiapia,^{†,‡} Alessandro Pezzella,^{*,†} Richard K. Heenan,[§] Aurel Radulescu,^{||} Luigi Paduano,^{†,‡} and Marco d'Ischia[†]

[†]Department of Chemical Sciences, University of Naples "Federico II", Via Cintia, 80126 Napoli (NA), Italy

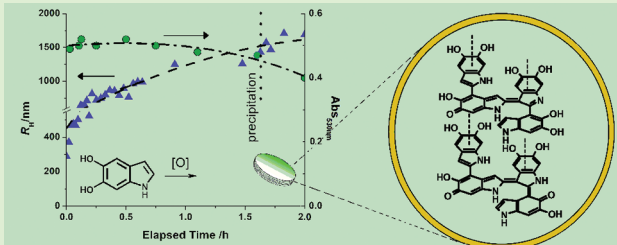
[‡]CSGI: Department of Chemistry, University of Florence, Via della Lastruccia 3, 50019 Sesto Fiorentino (FI), Italy

[§]ISIS-STFC, Rutherford Appleton Laboratory, Chilton, Oxon OX11 0QX, United Kingdom

^{||}Jülich Centre for Neutron Science, Lichtenbergstrasse 1, 85747 Garching, Germany

S Supporting Information

ABSTRACT: Establishing structure–property relationships in the black insoluble eumelanins, the key determinants of human pigmentation and skin photoprotective system, is a considerable conceptual and experimental challenge in the current drive for elucidation of the biological roles of these biopolymers and their application as advanced materials for organoelectronics. Herein, we report a new breakthrough toward this goal by the first detailed investigation on the nanoscale level of the oxidative polymerization of 5,6-dihydroxyindole (DHI), a model process of eumelanin synthesis. On the basis of a combined use of spectrophotometry, dynamic light scattering (DLS), and small-angle neutron scattering (SANS) investigations, it was possible to unveil the dynamics of the aggregation process before precipitation, the key relationships with visible light absorption and the shape of fundamental aggregates. The results indicated a polymerization mechanism of the type: $\text{Polymer}_n + \text{DHI}_x = \text{Polymer}_{n+x}$ where DHI_x indicates monomer, dimer, or low oligomers ($x \leq 5$). During polymerization, visible absorption increases rapidly, reaching a plateau. Particle growth proceeds slowly, with formation of 2-D structures ~ 55 nm thick, until precipitation occurs, that is, when large aggregates with a maximum hydrodynamic radius (R_h) of ~ 1200 nm are formed. Notably, markedly smaller R_h values, up to ~ 110 nm, were determined in the presence of poly(vinyl alcohol) (PVA) that was shown to be an efficient aggregation-preventing agent for polymerizing DHI ensuring water solubilization. Finally, it is shown that DHI monomer can be efficiently and partially irreversibly depleted from aqueous solutions by the addition of eumelanin suspensions. This behavior is suggested to reflect oxidant-independent competing pathways of polymer synthesis and buildup *via* monomer conversion on the active aggregate surface contributing to particle growth. Besides filling crucial gaps in DHI polymerization, these results support the attractive hypothesis that eumelanins may behave as a peculiar example of living biopolymers. The potential of PVA as a powerful tool for solution chemistry-based investigations of eumelanin supramolecular organization and for technological manipulation purposes is underscored.



INTRODUCTION

Eumelanins, the black insoluble biopolymers of human skin, hair, and eyes, have been the focus of unabated research interest at a multidisciplinary level over almost a century, following the discovery of their biogenetic origin from *L*-tyrosine or DOPA (3,4-dihydroxy-*L*-phenylalanine) *via* the oxidative polymerization of 5,6-dihydroxyindole (DHI) and related compounds (Scheme 1).^{1–4}

However, despite continuing efforts over the past two decades, the basic mechanisms of buildup of these biopolymers and the origin and features of their supramolecular architecture have remained largely obscure, mainly due to the marked insolubility and chemical heterogeneity of these pigments, making their investigation a most challenging task.^{4–7}

Direct experimental investigations of eumelanin samples of different origin using complementary techniques,^{8–12} coupled to theoretical studies,^{13–15} suggested that the polymer is composed of stacked layers of oligomeric, planar proto-entities (four to six indolic moieties)⁶ with spacings characteristic of π – π interactions. In fact, most of these early structural studies were developed around the hypothesis¹⁶ of the existence of fundamental aggregates steering the buildup of the larger final structures composing eumelanin particles.

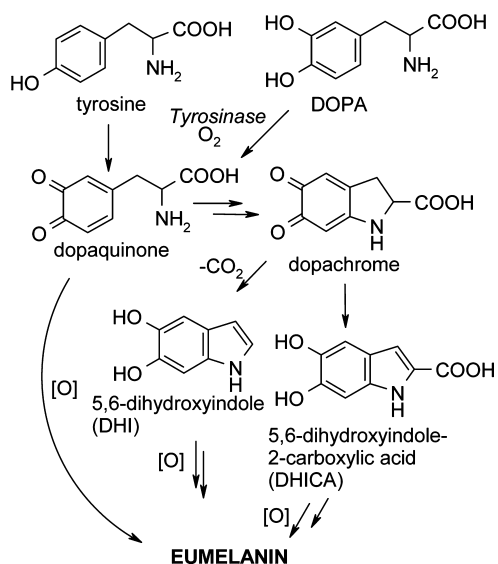
Some insights into the mechanisms and dynamics of eumelanin self-assembly and aggregation were gained by

Received: April 23, 2012

Revised: May 31, 2012

Published: May 31, 2012

Scheme 1. Schematic Outline of Eumelanin Synthesis



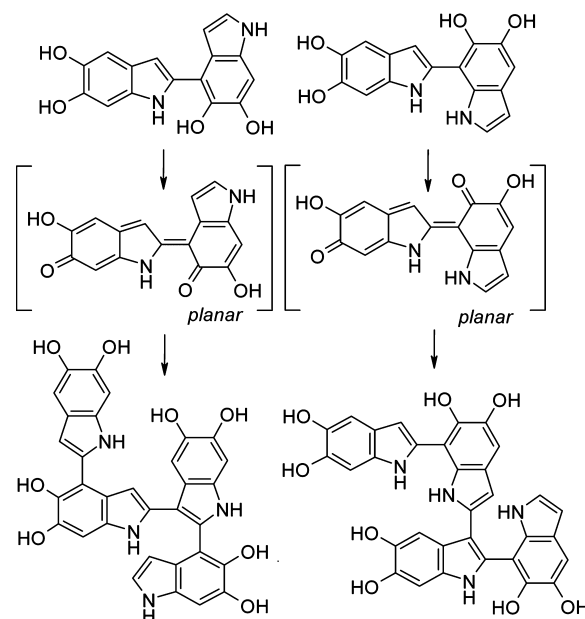
scattering techniques. Studies of synthetic melanin synthesis from DOPA in acidic aqueous solution (pH 2 to 3)¹⁷ indicated two regimes of aggregation, an initial Diffusion-Limited Aggregation (DLA) in which the particles stick on contact, characterized by clusters with fractal dimension $d = 1.8$, and a subsequent Reaction-Limited Aggregation (RLA) in which the particles stick only after multiple collisions, with aggregates at $d = 2.2$. Subsequent analysis of autooxidative and enzymatically produced DOPA eumelanin samples suggested that synthetic melanins grow as fractal aggregates of small units, following the DLA or RLA kinetics depending on the medium conditions.¹⁸ The fractal organization of eumelanins was supported by different approaches, including an analysis of nitrogen adsorption isotherms.¹⁹

Model studies of the oxidative polymerization of DHIs under biomimetic conditions provided important information on the nature of the oligomer intermediates leading to eumelanin formation.^{20–25} Especially worthy of note is the main mode of coupling of DHI and its dimers *via* the two-position of the indole ring (Scheme 2).

Pulse radiolysis and computational investigations of quinonoid species from DHI-derived biindoles showed that these can adopt planar structures (see, for example, Scheme 2), which can generate intense visible chromophores.²¹ Mass spectrometric studies on natural and synthetic eumelanins^{26–28} as well as on DHI polymerization processes^{5,29} indicated relatively low-molecular-weight oligomer species with partial structural degradation.

Considerable uncertainties still surround the origin of eumelanin “black chromophore”. According to the “chemical disorder” model,³⁰ which conveys little or no structural definition, eumelanins are collections of structurally diverse molecular species with overlapping chromophores covering the entire UV–visible range. Recently, the development of the first water-soluble DHI-based polymer allowed showing that the eumelanin “black chromophore” is defined not only by the conjugation length of the isolated absorbing species³¹ (“intrinsic” chromophore component) but also by the external perturbation of chromophores following intermolecular interactions and aggregation (“extrinsic” component).³¹ Support to this view came from the discovery that poly(vinyl alcohol)

Scheme 2. Structures of Representative Oligomers of DHI and Oxidized Species Thereof



(PVA), a well-known hydrophilic polymer, can prevent the precipitation of the growing melanin polymer during DHI oxidation.³¹ By this approach, it was possible to demonstrate that visible chromophore development during the early oligomer stages is independent of precipitation phenomena.

Despite these and other recent advances, a number of crucial gaps still hinder an understanding of the formation process and supramolecular organization of natural and synthetic eumelanin polymers and their relationships to the intriguing broadband absorption. Specific issues that remained to be addressed include: (i) the actual mechanism of DHI polymer growth (e.g., *via* a monomer–oligomer sequence or by oligomer–oligomer couplings); (ii) the average size distribution and shape of the initially formed molecular species prior to precipitation; (iii) the relative contribution of covalent versus noncovalent mechanisms during the early steps of polymerization; and (iv) the relationships between polymer growth, aggregate assembly, and visible chromophore development. Filling these gaps is essential to dispel current uncertainties concerning the biological roles and photoprotective functions of these biopolymers and to orient ongoing research aimed to meet the growing demand for rationally designed bioinspired functional materials for application in organoelectronics or as radioprotectors.³¹ Knowing and being able to control the aggregation processes in growing DHI polymers is moreover an essential goal in the prospects of transferring the unique physical properties of eumelanin-like polymers into applications.

Herein, we describe the successful elucidation of crucial aspects of the oxidative polymerization of DHI, including the mechanisms of particle buildup and underlying aggregation dynamics, by a bottom-up approach including a combined dynamic light scattering (DLS) and small-angle neutron scattering (SANS) analysis.

EXPERIMENTAL SECTION

DHI was synthesized as previously reported.³² Oxidation of DHI in 0.1 M phosphate buffer pH 7.0 was carried out with the substrate at 12.5

mM using horseradish peroxidase (HRP) (25 U/mL) and H₂O₂ (12.5 mM), and after 20 min the solution was diluted 25–100 times with 0.1 M phosphate buffer pH 7.0;³³ the spectrum was recorded in a thermostated cell at 298 K with or without filtration through a membrane with 0.47 L pores. When necessary, the mixture was treated with a solution of NaBH₄ in water (20 mM). DHI was also used at 12.5 mM, and after 20 min spectra were taken on the solution after separation of the pigment. In PVA-added medium, the buffers used were prepared by dissolving PVA in the appropriate weight ratio and warming to prevent cluster formation. Prior to oxidations, buffers were then thermostated at the desired temperature.

Absorption spectra were recorded on a spectrophotometer having the cell compartment thermostated at (25.0 ± 0.2) °C. Ultraviolet–visible (UV–vis) absorption spectra were recorded using a Jasco V 560 diode array spectrophotometer. Absorption behavior was monitored at 530 nm, where the absorbance of DHI markedly depends on its aggregation state.³⁴ Mass spectra were registered in ESI+ mode with the cone and the fragmentator voltage set at 4 kV and 80 V, respectively. ¹H and ¹³C NMR spectra were recorded at 400 and 300 MHz, respectively. Analytical and preparative TLC was carried out on silica gel plates (0.25 and 0.50 mm, respectively) from Merck. HPLC analysis of the reaction mixtures was carried out on a Gilson apparatus equipped with a UV detector set at 280 nm using a Spherclone ODS (5 μm, 4.6 × 250 mm) column. 1% vol/vol acetic acid/acetonitrile 95:5 (v/v) (eluant A) and acetonitrile (eluant B) gradients were used as follows: 0–5 min 30% eluant B, 5–40 min 30–80% eluant B, and 40–50 min 80% eluant B (flow rate of 1 mL/min). Centrifugations were performed with a Beckman Avant J-25 centrifuge.

Dynamic Light Scattering Measurements. DLS investigations were performed with a setup composed of a Photocor compact goniometer, an SMD 6000 Laser Quantum 50 mW light source operating at 5325 Å and a PMT-120-OP/B, and a correlator (Flex02-01D) purchased from Correlator.com. All measurements were performed at (25.00 ± 0.05) °C with the temperature controlled through the use of a thermostat bath. In DLS, the intensity autocorrelation function $g^{(2)}(t)$ is measured and related to the electric field autocorrelation function $g^{(1)}(t)$ by the Siegert relation³⁵

$$g^{(2)}(t) = 1 + \beta |g^{(1)}(t)|^2 \quad (1)$$

where β is the coherence factor, which accounts for the deviation from ideal correlation and depends on the experimental geometry. The function $g^{(1)}(t)$ can be written as the Laplace transform of the distribution of the relaxation rates, Γ , used to calculate the translational diffusion coefficient, D

$$g^{(1)}(t) = \int_{-\infty}^{+\infty} \tau A(\tau) \exp\left(-\frac{t}{\tau}\right) d \ln \tau \quad (2)$$

where $\tau = 1/\Gamma$. Laplace transforms were performed using a variation of CONTIN algorithm incorporated in Precision Deconvolve software. From the relaxation rates, the diffusion coefficient D may be obtained as

$$D = \frac{\Gamma}{q^2} \quad (3)$$

where $q = 4\pi n/\lambda \sin(\theta/2)$ is the modulus of the scattering vector, n is the refractive index of the solution, λ is the incident wavelength, and θ represents the scattering angle.

Provided that the solutions are quite dilute, the Stokes–Einstein equation,³⁶ which rigorously holds at infinite dilution for spherical species diffusing in a continuous medium, may legitimately be used to evaluate the hydrodynamic radius R_h of the aggregates

$$R_h = \frac{kT}{6\pi\eta D} \quad (4)$$

where k is the Boltzmann constant, T is the absolute temperature, and η is the medium viscosity. For nonspherical particles, R_h in eq 4 represents the radius of equivalent spherical aggregates with the same diffusion coefficient.

Because of the time evolution of the polymer growth, acquisition time of each measurement was set as a compromise between a good data statistics (that requires long accumulation times) and a reasonable snapshot of the system (that needs for short accumulation times).

Small-Angle Neutron Scattering Measurements. SANS measurements were performed at 25 °C with the KWS2 instrument of Jülich Centre for Neutron Science (JCNS) located at the research neutron source “Heinz Maier-Leibnitz” (FRM II) in Garching (Germany) and at the SANS2D instrument sited at the ISIS facility of the Rutherford Appleton Laboratory of Chilton (United Kingdom). In the first case, monochromatized neutrons with a wavelength spread $\Delta\lambda/\lambda \leq 0.2$ were used. A 2-D 128 × 128 array scintillation detector at three different wavelength (W)/collimation (C)/sample-to-detector (D) distances ($W_{7\text{Å}}C_{8\text{m}}D_{2\text{m}}$, $W_{7\text{Å}}C_{8\text{m}}D_{8\text{m}}$, and $W_{19\text{Å}}C_{8\text{m}}D_{2\text{m}}$) was used. These configurations allowed collection of scattering cross sections in an interval of scattering vector modulus $q = 4\pi/\lambda \sin(\theta/2)$ between 0.002 and 0.17 Å⁻¹, where θ is the scattering angle. Detector efficiency corrections and transformation to absolute scattering cross sections $d\Sigma/d\Omega$ were made with a secondary plexiglass standard, according to the procedure described elsewhere.³⁷

At the ISIS facility, pulsed neutron source SANS2D used neutrons of wavelengths between 2 and 14 Å detected by a time-of-flight analysis on a 98 cm² 2-D detector placed at 8 m from the sample, and the detector was offset sideways by 0.22 m and vertically by 0.15 m giving a q range of 0.003 to 0.33 Å⁻¹. Raw data were corrected for wavelength-dependent sample transmissions, incident spectrum, and detector efficiency and then transformed in absolute scattering cross-section $d\Sigma/d\Omega$ by comparison with scattering from a partially deuterated polystyrene standard.

Experimental Procedure for DLS and SANS Experiments. For DLS investigations, the oxidative process of DHI (at 0.1 mM concentration) was carried out in 0.1 M phosphate buffer (pH 7.0) under two different conditions: (1) with peroxidase/H₂O₂ and (2) by using dissolved O₂ as oxidant, in the presence of tyrosinase as enzyme. In both cases, systems were studied both in the absence and in the presence of PVA at various concentrations. To stop the oxidation and obtain a snapshot of the system, some selected systems were analyzed by adding, at suitable elapsed times, 100 equiv of sodium dithionite as polymer growth inhibitor.

More concentrated DHI samples (2.0 mM) with tyrosinase/O₂ were analyzed in SANS experiments, both in the absence and in the presence of PVA at various concentrations.

RESULTS AND DISCUSSION

Although previous studies used scattering techniques to address the origin of eumelanin polymers in terms of fundamental aggregates and their supramolecular organization,¹⁸ in most instances, the approach was based on the analysis of preformed polymers prepared under different and often incomparable conditions. Use of tyrosine or DOPA as the substrates, in particular, may lead to relatively heterogeneous materials with variable unit composition. Oxidation of these early biogenetic precursors proceeds *via* a notoriously complex polymerization pathway that involves an interplay of strictly interrelated steps profoundly susceptible to changes in the experimental conditions, whereby the process of particle growth can follow several different competing routes yet. As a result, the relative ratios of DHI building blocks and other monomer units that concur to polymer formation may change significantly, with a consequent increase in structural complexity and poor reproducibility.

The present study was conceived with a view of dissecting those crucial steps of eumelanin buildup that specifically relate to the oxidative polymerization of DHI, one of the key ultimate monomer precursors along with the 2-carboxylic acid. Use of the indole building block in the place of the early biogenetic precursors offered several important advantages, including

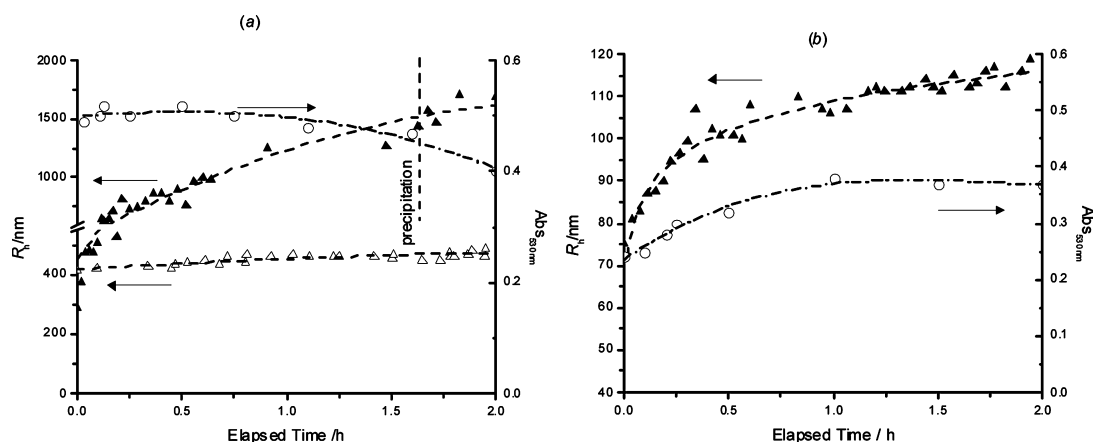


Figure 1. Hydrodynamic radii R_h (\blacktriangle) and absorbances measured at 530 nm (\circ) for the oxidative process of DHI with peroxidase/ H_2O_2 in phosphate buffer in the absence (on the left) and in the presence (on the right) of 0.1 wt % PVA. R_h values obtained for the oxidative process of DHI with in the presence of 100 equiv sodium dithionite are also reported (\triangle , on the left side).

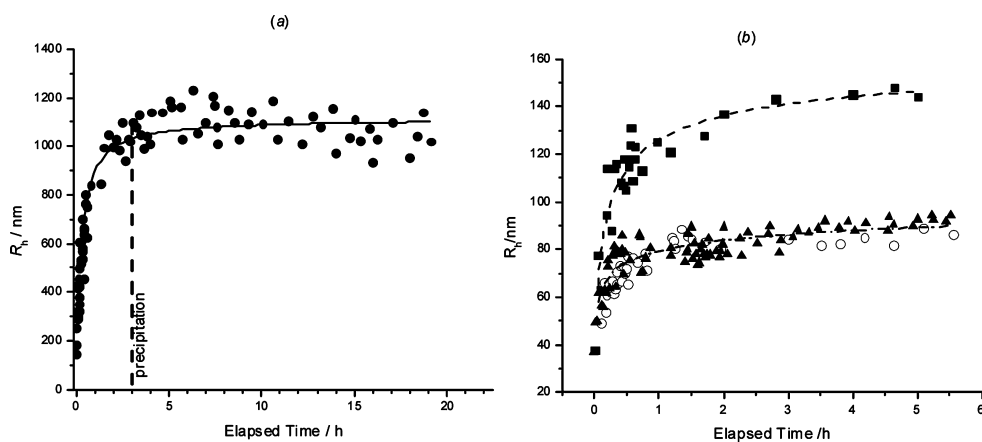


Figure 2. Hydrodynamic radii obtained by means of DLS technique for the oxidative process of DHI with tyrosinase in phosphate buffer in the absence (a) and in the presence (b) of 0.01 (\blacksquare), 0.05 (\blacktriangle), and 0.1 wt % (\circ) of PVA.

circumvention of competing pathways preceding the branching point of dopachrome rearrangement³⁸ (Scheme 1) and chemically more homogeneous reaction mixtures, consisting exclusively of indole-based oligomers. When carried out under typical biomimetic conditions, for example, in phosphate buffer at pH 7.4 in the presence of HRP/ H_2O_2 or tyrosinase, oxidation of DHI results in the rapid development of a dark coloration, followed by precipitation of black eumelanin-like polymers. Whereas use of these oxidants is commonly reported for polymerization studies, selection of reaction conditions was not straightforward and was adapted to the specific experimental requirements of the various analytical techniques. For example, the development of dark colored species during DHI polymerization critically affected DLS measurements due to the decrease in incident light intensity by absorption. Accordingly, in all DLS experiments (see below), DHI oxidation was investigated at a substrate concentration of 0.1 mM, under which conditions absorption effects were not critical and reaction rates were suitable for obtaining “snapshots” of the system.

Dynamic Light Scattering. Figure 1 shows the time evolution of the hydrodynamic radius (R_h) of DHI oxidation products upon the addition of peroxidase/ H_2O_2 in the absence (panel a) and in the presence (panel b) of 0.1 wt % PVA as a polymer solubilizing agent.

In the absence of PVA, soon after the addition of the oxidizing system, for example, at 1 min reaction time, the R_h value was ~ 300 nm, growing steadily up to ~ 1200 – 1300 nm after 1 h and reaching ~ 1500 nm after 2 h. In this latter time range, the formation of small black particles was detected. Therefore, these R_h values represent the maximum apparent size attainable by the growing polymer before precipitation. The addition of sodium dithionite to the oxidation mixture markedly slowed down the particle growth process, without modifying the size aggregates, as can be observed in Figure 1a. A plot of the absorbance at 530 nm with time showed the generation, already at 1 min, of an intense visible chromophore that remained stable as a plateau before decreasing after ~ 1 h due to incoming precipitation.

In the presence of 0.1 wt % PVA, a marked inhibition on eumelanin polymer growth was noted (Figure 1b), leading to a R_h value of only 110 nm after 1 h of reaction time, without apparent precipitation. Interestingly, absorbance determination at 530 nm with time revealed again the immediate development of a visible chromophore, which, however, was less intense and did not level off, as in panel a, but increased smoothly by an additional 40% plateauing not earlier than ~ 1 h. Comparative analysis of these data would suggest that PVA entraps the growing polymer particles and prevents them from further

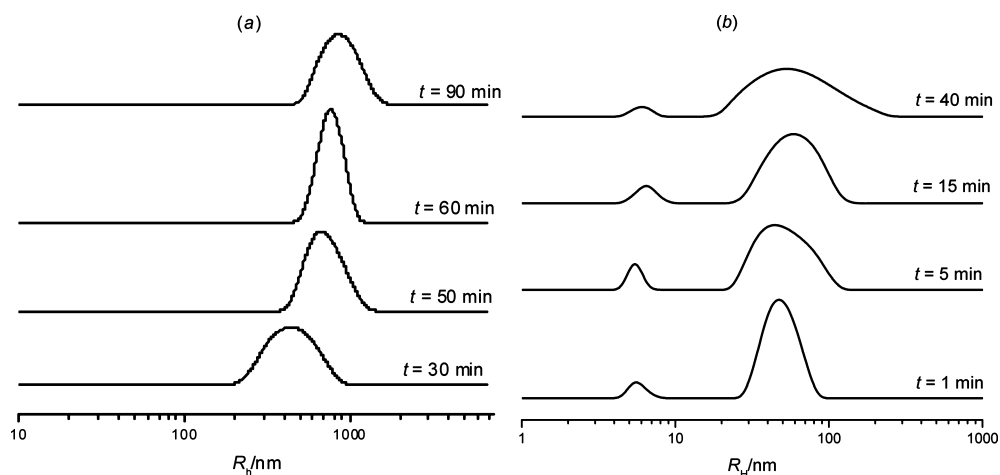


Figure 3. Hydrodynamic radius distribution functions measured at 90° for various elapsed times for the oxidative process of DHI with tyrosinase in phosphate buffer in the absence (a) and in the presence (b) of 0.5 wt % PVA.

increase, probably by posing physical constraints to covalent bonding or aggregation.

In another series of experiments, the oxidation of DHI was carried out as above but in the presence of tyrosinase, under which conditions the oxidative polymerization proceeded at slower pace. Data in Figure 2 (panel a) indicated again a maximum R_h value of ~ 1200 nm before detectable polymer precipitation, which occurred not earlier than 3 h of reaction time.

It is interesting to note a substantial difference existing among the assembly mechanism occurring in DHI solutions at physiological values and the one found by Huang that involves two different regimes.¹⁷ In the present case, according also to the simple kinetic model developed, only a RLA regime is observed, in which the molecular reactivity slows down as long the polymeric adduct progressively increases.

In the presence of 0.1 wt % PVA, the R_h value increased from an initial value of ~ 30 to ~ 100 nm over 5 h (Figure 2b). Small aggregates were detected at the very beginning of the reaction due to the slower reaction rate with respect to the peroxidase/ H_2O_2 conditions.

The effects of varying PVA concentration (0.01 to 0.5 wt %) on the tyrosinase-promoted polymerization were next investigated (Figure 2, panel b). Complete inhibition of polymer growth was observed even at the lowest additive concentration. Increasing PVA concentrations resulted in slower kinetics of polymer growth with a decrease in the hydrodynamic radius of the aggregates by at least one order of magnitude with respect to the normal process in the absence of PVA. However, it is to note that above PVA 0.05 wt % no differences were detected in the DHI kinetic growth.

In all DLS experiments, only a single R_h distribution was detected in PVA-free systems. (The aggregate distribution is monomodal, as can be observed in Figure 3a.) In the presence of PVA, two aggregate populations are detected, the first corresponding to the PVA presence ($R_h \approx 5$ to 6 nm) and the second distribution attributable to the eumelanin aggregates (Figure 3b). The invariant value of the hydrodynamic radius as well as its size distribution suggests that PVA does not interact significantly with DHI-derived growing polymer.

The lack of detectable species of intermediate molecular size throughout the entire polymerization process and the finding that most of the hydrodynamic radius values fall within 30% of

the mean R_h value are both consistent with a relatively regular polymer growth mechanism involving sequential coupling processes of the monomer–polymer type rather than oligomer–polymer or polymer–polymer couplings.

A question then arose of what model could fit the above data in the advanced stages of the process, when most of the starting monomer is consumed. To address this issue, the oxidative polymerization of a dimer of DHI, namely, the 2,7'-biindole, was investigated to assess whether the kinetics and overall features of the polymerization process, including R_h distribution with growing polymer, matched those observed during monomer oxidation. The results reported in Figure 4 indicated

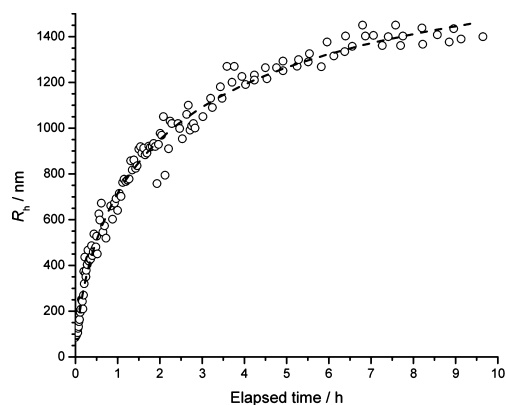


Figure 4. Hydrodynamic radii obtained by means of DLS technique for the oxidative process of 2,7'-biindole with tyrosinase in phosphate buffer.

that monomer and dimer polymerization proceed with quite similar features, suggesting similar oxidative coupling mechanisms. It is, however, apparent that the scattering technique cannot distinguish between the monomer and dimers or, possibly, low-molecular-weight oligomers, so, in principle, all of the initially formed low-molecular-weight species, within a low mass limit, can take part in the polymerization. On this basis, it appears that the process involves initially the addition of monomer units to the growing polymer but in the subsequent stages, when monomer levels decrease, the lower oligomers, for example, dimers, trimers, and so on, sustain polymer growth.

Small-Angle Neutron Scattering. Whereas DLS data provided insight into the size distribution profile of the growing oligomers and the effects of PVA, information about the morphology and the structural parameters of the growing DHI polymer was sought using SANS (Figure 5). Measurements in

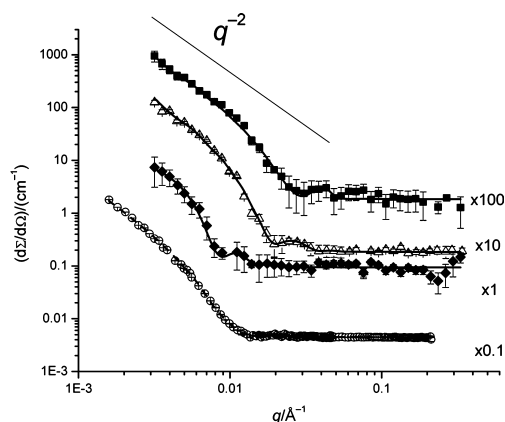


Figure 5. Scattering cross sections obtained for DHI with tyrosinase 2.0 mM in phosphate buffer at pH 7.4 in the absence (○) and in the presence of PVA at 0.5 (◆), 1.0 (△), and 1.5 wt % (■). The measurements in the presence of PVA have been performed in a D₂O/H₂O mixture such to mask the PVA scattering, as described in the text. PVA-free system has been analyzed in D₂O. Solid lines represent the fitting curves obtained from the application of the model described in the text. To allow for a better visualization, scattering cross sections have been multiplied for a scale factor, as indicated.

the absence of PVA were performed in a deuterated phosphate buffer to minimize the incoherent scattering contribution to the total cross section. In the presence of PVA polymer, a suitable H₂O/D₂O mixture ($x_{\text{H}_2\text{O}} = 0.816$ and $x_{\text{D}_2\text{O}} = 0.184$ molar fractions) was used to mask scattering arising from polymer and selectively analyze DHI aggregates.³⁹ In all cases, DHI substrate concentration was increased with respect to the DLS experiments to allow for reliable acquisition of data under the specific instrumental conditions due to the lower sensitivity of SANS with respect to DLS.

PVA-free system was analyzed just after 20 min from the system preparation, that is, after the addition of tyrosinase, whereas systems containing PVA were analyzed after 24 h, to ensure that the oxidation process was complete. We note that due to the rapid time evolution occurring in the absence of PVA measurement duration was ~15 min long, hence well before precipitation phenomenon. Inspection of Figure 5 indicated a power law of -2 for the decay of the scattering cross section $d\Sigma/d\Omega$ vs the scattering vector modulus, q , which is consistent with large 2-D structures, such as bilayers or discs. Inspection of the scattering intensity profile did not reveal any peak or shoulder in the intermediate q range (0.02 to 0.04 \AA^{-1}) that would suggest the presence of detectable small aggregates. This observation is in agreement with the DLS results and concurs to rule out the absence of small oligomers ($<10 \text{ nm}$) during the reaction progress. Omitting or varying PVA percentage from 0.5 to 1.5 wt % did not cause any significant change in the essential characteristics of the polymer intermediates.

More detailed interpretations were obtained using the length Schulz polydisperse disk model.⁴⁰ If r and d represent the disk

radius and thickness, then for such a model scattering cross sections $d\Sigma/d\Omega$ can be written as

$$\frac{d\Sigma}{d\Omega} = k \int_0^{+\infty} f(d)P(q, r, d) dr + \left(\frac{d\Sigma}{d\Omega}\right)_{\text{incoh}}$$

where $f(d)$ is the normalized Schulz distribution function of the thickness

$$f(d) = \left(\frac{Z+1}{\bar{d}}\right)^{Z+1} \frac{x^Z}{\Gamma(Z+1)} \cdot \exp\left(-\frac{Z+1}{\bar{d}}d\right)$$

$P(q, r, d)$ is the normalized form factor of a disk and k represents a proportionality factor depending on the disk particle density and scattering contrast. Finally, $(d\Sigma/d\Omega)_{\text{incoh}}$ is the incoherent contribution to the total scattering cross sections, mainly due to the presence of hydrogenated molecules. In the Schulz distribution function, \bar{d} represents the average disk thickness, whereas Z is a parameter that takes into account the polydispersity index $i_d = 1/(Z+1)$.

Indeed, the randomly oriented planar sheet model⁴¹ and the monodisperse disk model⁴⁰ were also examined, but the polydisperse length disk model allowed having better results in terms of χ^2 parameter, as reported in Figure S1 of the Supporting Information, except for the PVA-free system, where the disk length polydispersity has been observed to be negligible if compared with systems containing PVA.

From the model, the disk thickness d was obtained, along with its polydispersity i_d , as detailed in Table S1 of the Supporting Information. It is worthy to note that the lack of Guinier regime for all the measurements did not allow getting the disk radius, whose estimation would require data in the USANS domain.

Disc thickness d estimated through the fitting was ranged from $(55 \pm 2) \text{ nm}$ for the system PVA-free to $(21 \pm 2) \text{ nm}$ in the presence of PVA 1.5 wt %. At 1.0 wt % of this polymer, an intermediate value of $(33 \pm 1) \text{ nm}$ was obtained. The calculated values determine the maximum q_{max} where the q^{-2} power law dependence still occurs, that is, $q_{\text{max}} = 2\pi/d$.⁴⁰

The thickness values found would suggest a spatial disposition in which planar oligomer structures interact to form typical more-or-less regular π stacks (Figure 6). Assuming typical spacing in the order of 3.4 \AA , it can be deduced that each aggregate would contain many tenths of planar oligomer structures.

Reduction of transversal thickness d observed with the increasing of PVA content is coupled to a decrease in

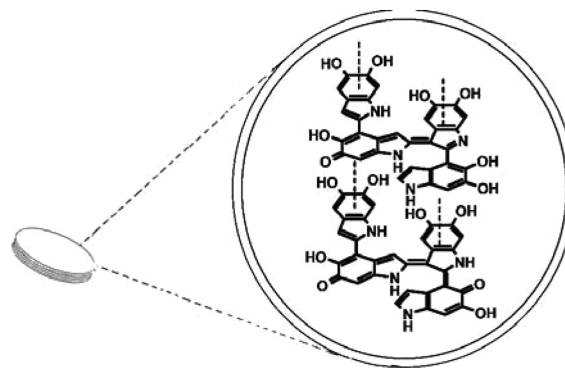


Figure 6. Schematic representation of the fundamental aggregate as inferred from SANS data.

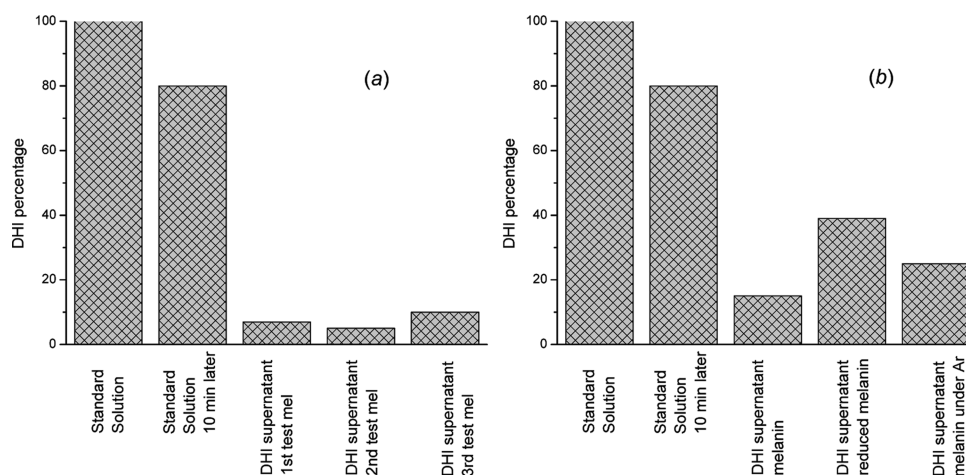


Figure 7. (a) DHI recovery from eumelanin suspensions and (b) after reduction.

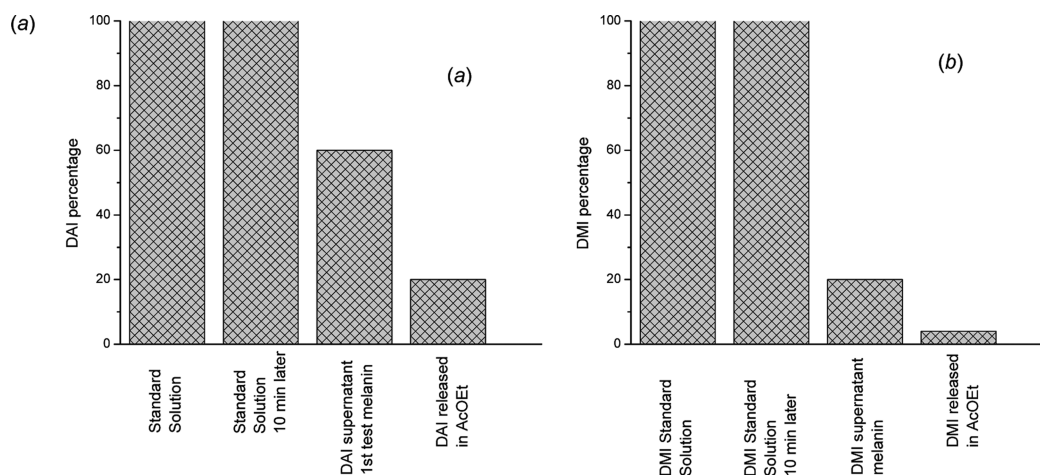


Figure 8. (a) DAI and (b) DMI recovery from eumelanin suspensions.

polydispersity of this parameter: this confirms that PVA does not directly interact with polymer growth, but its role seems limited to the creation of a cage thwarting DHI adduct growth, at least along the two main dimensions. In other words, it acts through an excluded volume effect^{42,43} by confining the polymer growth in a restricted region. Indeed, such behavior has already been observed in PVA-containing systems in the presence of micelle aggregates. There, the micellar structure was not influenced by the presence of PVA; only a marked decrease in aggregate diffusivity was detected.³⁹

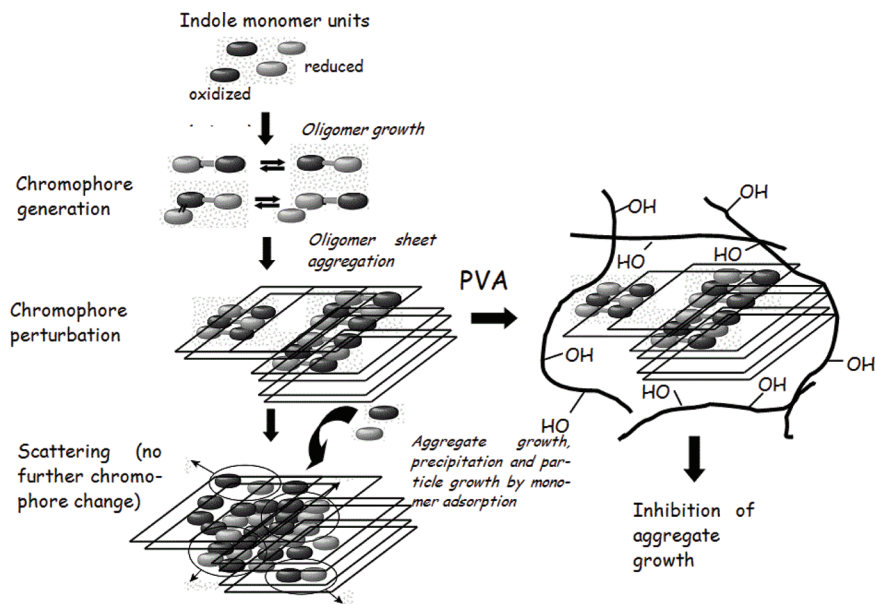
DHI–Eumelanin Interactions. The results of the above experiments concurred to support a polymerization model in which monomer and low-molecular-weight units are rapidly consumed by coupling to the larger growing entities. Although these steps are oxidative in character, it seemed of interest to assess whether adsorption mechanisms independent of solution-phase oxidative coupling play any role in particle buildup during the later stages after precipitation has initiated. To this aim, subsequent experiments were directed to determine whether DHI can interact with the eumelanin polymer in the absence of added oxidants and whether this interaction is reversible. When a DHI eumelanin, obtained as previously reported,³³ was finely suspended into a freshly prepared solution of DHI at 2 mM concentration in phosphate buffer pH 7.4, a relatively rapid drop in indole concentration occurred, as determined by HPLC analysis of the supernatant

following periodical centrifugation of aliquots of the mixture to remove the suspended solid (Figure 7). These data are the first to demonstrate that eumelanin monomer precursors can be efficiently adsorbed onto the solid polymer in the absence of external oxidants.

Repetition of the same procedure using the finely suspended polymer recovered from the mixture gave similar results, which were confirmed at least after three cycles of adsorption recovery, suggesting that iterating monomer adsorption does not affect the binding ability of the synthetic eumelanin. Interestingly, a significant decrease in the extent of DHI adsorption was noted under an argon atmosphere or pretreating the DHI eumelanin with sodium dithionite as reducing agent, suggesting that oxidation processes on the surface of the eumelanin particles play a role. When a eumelanin sample recovered after repeated exposures to DHI was stirred in MeOH for at least 10 min, HPLC analysis of the filtrate indicated that only a small amount of DHI, not exceeding 10% of the initial concentration, could be released in the medium. Slightly higher DHI levels were released from the samples obtained under an argon atmosphere or following reductive treatment with sodium dithionite.

To determine whether redox processes are involved in DHI binding to eumelanin polymer, the interactions of catechol-protected DHI derivatives, namely, 5,6-diacetoxyindole (DAI)

Scheme 3. Summarizing View of the Proposed Mechanism of Polymerization of DHI and Aggregation



and 5,6-dimethoxyindole (DMI), with DHI eumelanin were next investigated (Figure 8).

Interestingly, a rapid decay of DMI was observed after 10 min in the presence of suspended eumelanin, indicating that oxidation processes at the susceptible catechol moiety are not primarily responsible for monomer–polymer interactions. A slower rate of decay was determined in the case of DAI. Detectable monomer release (20%) by treatment with EtOAc was noted only in the case of DAI, whereas DMI was completely retained by the polymer. It is possible that the higher affinity of DMI for the eumelanin polymer depends on the higher electron density imparted to the indole ring by the methoxy, relative to the acetoxy groups, but this remains speculative at present.

Overall, these preliminary results disclose the ability of synthetic DHI eumelanin to bind indole monomers tightly, a property that seems to have escaped the attention of previous workers. The process can be accounted for in terms of an efficient adsorption phenomenon that is partially reversible and that may be further driven to completion by the oxidizing properties of the polymer surface and the availability of oxygen. It is likely that under these latter conditions oxidation reactions on the particle surface lead to covalent coupling with exposed polymer endings and reactive sites of the aggregate. Clearly, further work is required to obtain more in-depth information on the DHI–eumelanin interaction and, particularly, to determine to what extent such adsorption phenomena take place also on the growing particles on the nanoscale prior to precipitation.

Improved Mechanistic Model for Polymer Growth and Particle Assembly. Altogether, the results reported above are compatible with a kinetic model of DHI polymerization based initially on sequential interactions between the monomer/low oligomers and the growing aggregates. During the very early stages, that is, until the monomer concentration is high, eq 5 would dominate the kinetics of polymer growth



with n varying throughout the entire polymerization range.

Gradually, as dimers, trimers, and low oligomers are formed, the growth process can be described by a more general equation of the type



where DHI_{m^*} is an ensemble of low-molecular-weight oligomers contributing to polymer growth. (Formally, we would have been able to indicate them as P_{m^*} .) The accurate evaluation of the whole distribution of m^* value is difficult, but the upper value is clearly set by the instrumental detection limits and is reasonably predicted to be low, for example, <5.

In the assumption that each step occurs with the same kinetic constant k , no matter of the species involved and in the absence of significant PVA–DHI interactions,⁴⁴ it is possible to derive an equation correlating the diffusion coefficient D to the kinetic characteristics of the process. The equation can be obtained considering momenta of the polymer size distribution according to an analysis reported elsewhere^{45,46}

$$\langle D \rangle = \frac{D_{\text{DHI}}(m^*N_a - c) \exp(-kN_a t) + D_a \left\{ \frac{1}{N_a} [(m^*N_a - c) \exp(-kN_a t) + c]^2 + (m^*N_a - c)(\exp(-kN_a t) - 1) \right\}}{(m^*N_a - c) \exp(-kN_a t) + \left\{ \frac{1}{N_a} [(m^*N_a - c) \exp(-kN_a t) + c]^2 + (m^*N_a - c)(\exp(-kN_a t) - 1) \right\}} \quad (7)$$

where c is the stoichiometric monomer concentration, D_{DHI} and D_a are the diffusion coefficients of DHI unimer and the final adduct, whereas N_a represents the molar concentration of polymer adducts.

On the basis of the above data, an improved model for the mechanism of polymerization of DHI is proposed (Scheme 3).

In this model, oligomer chains grow rapidly triggering fast and efficient aggregation processes. These result in the

formation of sheet-like aggregates up to a critical size limit. The relatively uniform R_h distribution suggests that aggregation occurs throughout the entire polymerization process, although it appears that the monomer and the dimers as well as the smaller oligomers, are the main species that sustain polymer growth.

Figure 9 shows the plots obtained through the fitting of eq 7 to the experimental data, and the fitting parameters are presented in Table S2 of the Supporting Information. Inspection of the Table suggests that small oligomers (with $m^* \approx 4$), formed in the early stages of the DHI oxidation

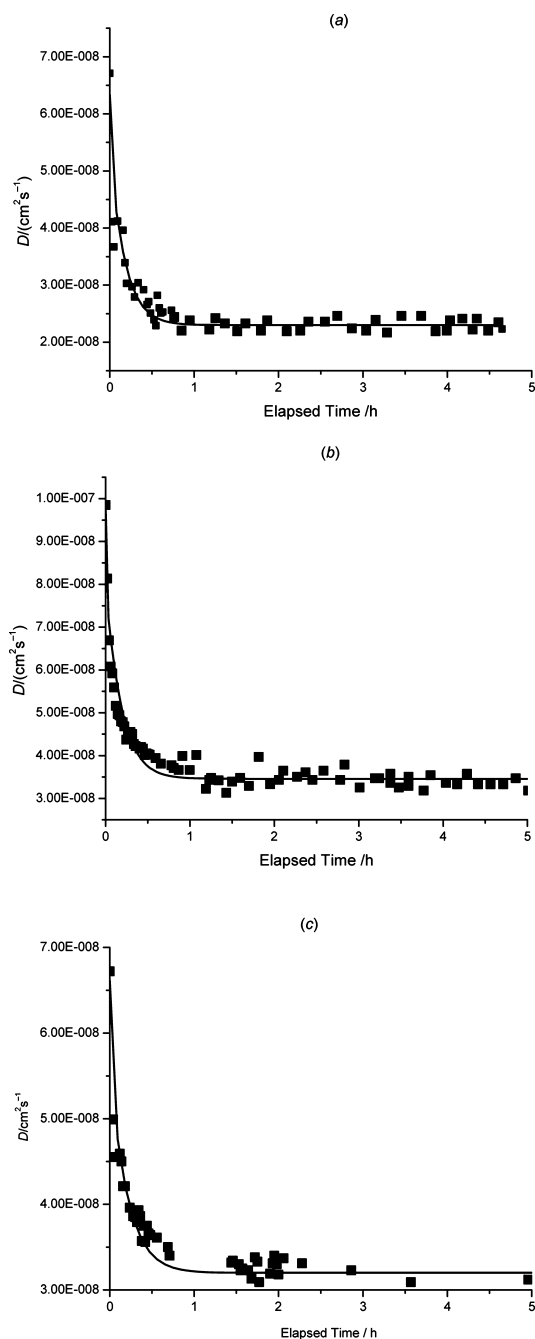


Figure 9. Diffusion coefficients measured by DLS experiments at 25 °C for DHI polymer growth in the presence of PVA at (a) 0.01, (b) 0.05, and (c) 0.1 wt %. DHI stoichiometric concentration was set to 0.1 mM.

process are the “seeds” from which the polymer growth originates.

A comparison of the present model with those of the previous studies on synthetic eumelanins discloses interesting aspects of synthetic relevance. As previously mentioned, in the early studies,^{17,18} measurements of the polymerization kinetics of self-oxidative and enzymatically prepared DOPA eumelanins samples showed different behaviors in the time evolution of the average dimensions of the granules that reflected different kinetic regimes with experimental conditions. Apparently, this was not the case with DHI polymerization. It is possible that this difference reflects the diverse chemical properties of DOPA and DHI oxidation products, whereby the lower solubility and early onset of precipitation in the case of DHI oligomers would favor a single regime, namely, that called RLA regime, dictated by the progressively reduced reactivity of the large polymeric adducts.^{17,18}

It should be emphasized, in this regard, that the kinetic model does not take into account whether polymer growth occurs by covalent bonding or whether adsorption and aggregation phenomena also play a role on the nanoscale because no data are available to support or rule out either of the two possibilities. Most likely, noncovalent aggregation processes are responsible for the large particles preceding precipitation in the absence of PVA, but detailed information is not yet available regarding the molecular weight limits of oligomer/polymer chains in DHI eumelanin. On the basis of previous mass spectrometric data of DHI polymers, ruling out very high-molecular-weight species,^{11,12,16,27,29,47,48} it can be speculated that growing oligomer/polymer chains rapidly aggregate to form small entities that then gradually increase in a relatively homogeneous fashion to form larger structures up to an apparent radius of ~ 1200 nm. These structures exist as apparently 2-D assemblies resembling graphene-like sheets or discs, reflecting preferentially edge-to-edge arrangements as in brickwork-type J-aggregates rather than parallel interactions as in π -stacked battery-like aggregates. In the presence of PVA, the initially formed aggregates would be physically entrapped within the entangling network of the hydrophilic polymer chains, thus being hindered from aggregation beyond a threshold size limit corresponding to R_h values of ~ 120 nm. This value is roughly comparable to the mesh size (~ 1000 nm) of the poor polymer phase present in PVA network formed through freeze/thaw process, suggesting a physical control over eumelanin particle growth. As a result, fine eumelanin aggregates of relatively uniform size are produced in the presence of PVA.^{39,42}

The visible absorption versus R_h profiles with time observed in the presence and in the absence of PVA (Figure 1) provide further insight into the origin and characteristics of eumelanin black chromophore. In the absence of PVA, absorbance at 530 nm attains its maximum value soon after DHI oxidation has started, indicating that visible chromophore development from the colorless DHI substrate occurs during the very early oxidation steps²¹ and does not proceed further despite continuing oligomer chain growth and aggregation. It is noted from Figure 1a that visible absorbance intensity plateaus when the particle hydrodynamic radius is still relatively small, in the range of 250–300 nm. The latter values would therefore indicate the apparent size of the “minimal eumelanin unit”, that is, the minimal particle size necessary to generate light-absorbing properties equivalent to those of a typical eumelanin-type polymer and beyond which no significant absorbance

increase occurs. In the presence of PVA, particle growth is severely constrained by the added polymer, which appears to efficiently hinder both oligomer chain elongation and aggregation processes. The main detectable consequence is a slower rate of visible chromophore plateauing associated with a lower absorbance value. It can be concluded that visible chromophore development in the presence of PVA follows a dual kinetic profile. Initially, a very fast process occurs, corresponding to DHI oxidation and formation of small colored quinonoid species (it should be noted here that even dimers are dark blue in color when oxidized),²¹ followed by a much slower one, in which visible absorption intensity increases modestly with increasing R_h . The early rapid increase in visible absorbance would thus denote the very fast generation of the oxidized low-molecular-weight population(s) responsible for visible light absorption. The slow process that then ensues would reflect two main factors: (a) the continuing increase in the population of the early low-molecular-weight chromophores as slowed down by the gradual monomer consumption, (b) the effect of growing oligomer chains on π -electron delocalization, and especially (c) intermolecular chromophore perturbation secondary to aggregation effects.³⁴ These latter effects, however, are not so pronounced as in the absence of PVA due to the hindering and tangling effect of added polymer. Overall, these observations are in line with the recently proposed chromophoric dynamic disorder model³⁴ and corroborate the view that eumelanin black chromophore reflects both an intrinsic component, due to the absorption properties of individual molecular constituents, and an extrinsic dynamic component, which refers to intermolecular interactions broadening intrinsic absorption bands and increasing visible light extinction.

The technological prospects of this size-controlling effect of PVA are manifold and would deserve further attention. The new information derived from this study would be most useful for the design of eumelanin-based nanostructured materials for technological applications. Further work is needed to identify the chemical structures of the molecular building blocks and thereby develop an understanding of the forces that govern the formation of the observed structures.

Finally, the demonstration in the present study that monomer units in solution can be strongly adsorbed by the solid eumelanin particles and that the adsorption, although partially dependent on the redox state of the polymer surface and the presence of oxygen, is largely irreversible opens new scenarios in the mechanisms of polymerization and aggregate formation. This phenomenon might entail hitherto unrecognized surface polymerization processes independent of external oxidants, which would impart a "living polymer"-like behavior to eumelanins, accounting for the generation of multilayered supramolecular aggregates once the solution phase polymerization processes preceding precipitation have been completed.¹⁰ In line with the conclusions from the previous study,¹⁸ it can be hypothesized that the direction of growth of the particles in DHI eumelanin is casual, as the granules are obtained by the addition of small units.

It is difficult at present to assess to what extent the results of this model study are relevant to the process of eumelanin synthesis *in vivo*. The organelle nature of melanosomes and the role of melanosomal proteins like Pmel 17 are critical in this regard.⁴⁹ Morphological investigations indicated that the molecular constituents of melanosome surface have a maximum spatial scale of ~ 10 nm and are held together by noncovalent

bonds. The presence of ~ 30 nm substructures in melanosomes from various sources was also established.⁵⁰ On this basis, it was argued that there is a hierarchy in the aggregation process *in vivo*, involving the generation of small fundamental aggregates that subsequently assemble into larger species *via* edge-to-edge or stacking interactions.^{8,12} On the basis of the present data, it can be concluded that such aggregation processes are of general relevance to eumelanin architecture and physicochemical properties both *in vitro* and *in vivo*.

CONCLUSIONS

Currently, there is no satisfactory theory describing the oligomer growth mechanisms and factors affecting aggregate assembly during DHI polymerization. In this Article, we have reported the first insight into this intriguing issue through a detailed analysis of the biomimetic process by two complementary scattering techniques. Several important results have been disclosed herein, which can be summarized as follows: (a) DHI polymers grow mainly *via* monomer–polymer or low oligomer–polymer coupling steps, rather than by large oligomer–oligomer interactions; (b) particle size increases steadily during polymerization with a very limited R_h dispersion; (c) the maximum apparent size attainable by aggregates before precipitation is ca. 1200 nm; (d) visible chromophore development reflects a dual component, an intrinsic one, and an extrinsic dynamic one, which account overall for the apparent lack of linear correlation with increasing particle size throughout the entire DHI polymerization process; (e) the fundamental aggregates look like 2-D planar sheets ~ 55 nm thick; and (f) DHI and related indole derivatives are strongly adsorbed onto DHI eumelanin suspensions even on repeated additions, suggesting a new concept of eumelanins as a peculiar case of living polymer.

Although the chemistry emerging from this study is an oversimplification of the actual complexity of the eumelanin assembly process *in vivo*, it provides new mechanistic paradigms of general relevance to the processes of polyphenol synthesis and opens the doorway to a more in-depth understanding of the structure–property–function relationships underpinning eumelanin biological roles and exploitation for practical applications. Another important outcome of this study is the potential of PVA for a solution chemistry approach to eumelanin growth and supramolecular organization. Used as an additive to the oxidation medium, PVA allows disentangling the overlapping effects of polymer chain growth, aggregate assembly, and visible chromophore development on pristine DHI-derived species without making recourse to functionalization. Considerable opportunities are anticipated by the development of PVA-based protocols as a strategy to control polymer size and aggregation for the engineering of tailored eumelanin-inspired functional materials.

ASSOCIATED CONTENT

Supporting Information

Information obtained from fitting of experimental data. This material is available free of charge via the Internet at <http://pubs.acs.org>.

AUTHOR INFORMATION

Corresponding Author

*E-mail: alessandro.pezzella@unina.it

Notes

The authors declare no competing financial interest.

ACKNOWLEDGMENTS

This work was carried out in the frame of the EuMelaNet project (<http://www.espcr.org/eumelanet/>). Financial support by MIUR, PRIN 2008 project, is gratefully acknowledged. We thank the Jülich Centre for Neutron Science and the Rutherford Appleton Laboratory for provision of beam time. SANS experiments were supported by the European Commission, NMI3 contract RII3-CT-2003-505925.

REFERENCES

- (1) Ito, S.; Wakamatsu, K., Chemistry of Melanins. In *The Pigmentary Systems Physiology and Pathophysiology*; Nordlund, J. J., Boissy, R. E., Hearing, V. J., King, R. A., Oetting, W. S., Ortonne, J. P., Eds.; Oxford Blackwell Publishing, Ltd.: Oxford, U.K., 2006; pp 282–310.
- (2) Prota, G. *Melanins and Melanogenesis*; Academic Press: San Diego, CA, 1992.
- (3) Simon, J. D.; Hong, L.; Peles, D. N. Insights into melanosomes and melanin from some interesting spatial and temporal properties. *J. Phys. Chem. B* **2008**, *112*, 13201–13217.
- (4) Simon, J. D.; Peles, D.; Wakamatsu, K.; Ito, S. Current challenges in understanding melanogenesis: bridging chemistry, biological control, morphology, and function. *Pigm. Cell Melanoma Res.* **2009**, *22*, 563–579.
- (5) Hatcher, L. Q.; Simon, J. D. Ultra-low temperature oxidation of 5,6-dihydroxyindole: a novel approach to study synthetic melanogenesis. *Photochem. Photobiol.* **2008**, *84*, 608–612.
- (6) Meredith, P.; Sarna, T. The physical and chemical properties of eumelanin. *Pigm. Cell Res.* **2006**, *19*, 572–594.
- (7) Simon, J. D.; Peles, D. N. The red and the black. *Acc. Chem. Res.* **2010**, *43*, 1452–1460.
- (8) Clancy, C. M. R.; Simon, J. D. Ultrastructural organization of eumelanin from sepia officinalis measured by atomic force microscopy. *Biochemistry* **2001**, *40*, 13353–13360.
- (9) Gallas, J. M.; Littrell, K. C.; Seifert, S.; Zajac, G. W.; Thiyagarajan, P. Solution structure of copper ion-induced molecular aggregates of tyrosine melanin. *Biophys. J.* **1999**, *77*, 1135–1142.
- (10) Watt, A. A. R.; Bothma, J. P.; Meredith, P. The supramolecular structure of melanin. *Soft Matter* **2009**, *5*, 3754–3760.
- (11) Cheng, J.; Moss, S. C.; Eisner, M.; Zschack, P. X-ray characterization of melanins-I. *Pigm. Cell Res.* **1994**, *7*, 255–262.
- (12) Zajac, G. W.; Gallas, J. M.; Cheng, J.; Eisner, M.; Moss, S. C.; Alvarado-Swaigood, A. E. The fundamental unit of synthetic melanin: a verification by tunneling microscopy of X-ray scattering results. *Biochim. Biophys. Acta, Gen. Subj.* **1994**, *1199*, 271–278.
- (13) Kaxiras, E.; Tsolakidis, A.; Zonios, G.; Meng, S. Structural model of eumelanin. *Phys. Rev. Lett.* **2006**, *97*, 218102/1–218102/4.
- (14) Stark, K. B.; Gallas, J. M.; Zajac, G. W.; Eisner, M.; Golab, J. T. Spectroscopic study and simulation from recent structural models for eumelanin: I. monomer, dimers. *J. Phys. Chem. B* **2003**, *107*, 3061–3067.
- (15) Stark, K. B.; Gallas, J. M.; Zajac, G. W.; Golab, J. T.; Gidanian, S.; McIntire, T.; Farmer, P. J. Effect of stacking and redox state on optical absorption spectra of melanins - comparison of theoretical and experimental results. *J. Phys. Chem. B* **2005**, *109*, 1970–1977.
- (16) Zeise, L.; Murr, B. L.; Chedekel, M. R. Melanin standard method: particle description. *Pigm. Cell Res.* **1992**, *5*, 132–142.
- (17) Huang, J. S.; Sung, J.; Eisner, M.; Moss, S. C.; Gallas, J. The fractal structure and the dynamics of aggregation of synthetic melanin in low pH aqueous solutions. *J. Chem. Phys.* **1989**, *90*, 25–29.
- (18) Bridelli, M. G. Self-assembly of melanin studied by laser light scattering. *Biophys. Chem.* **1998**, *73*, 227–239.
- (19) Crippa, P. R.; Giorcelli, C.; Zeise, L. Determination of surface characteristics and fractal dimensions of natural and synthetic eumelanins from nitrogen adsorption isotherms. *Langmuir* **2003**, *19*, 348–353.
- (20) d'Ischia, M.; Napolitano, A.; Pezzella, A.; Land, E. J.; Ramsden, C. A.; Riley, P. A. 5,6-Dihydroxyindoles and indole-5,6-diones. *Adv. Heterocycl. Chem.* **2005**, *89*, 1–63.
- (21) Pezzella, A.; Panzella, L.; Crescenzi, O.; Napolitano, A.; Navaratnam, S.; Edge, R.; Land, E. J.; Barone, V.; d'Ischia, M. Short-lived quinonoid species from 5,6-dihydroxyindole dimers en route to eumelanin polymers: integrated chemical, pulse radiolytic, and quantum mechanical investigation. *J. Am. Chem. Soc.* **2006**, *128*, 15490–15498.
- (22) Pezzella, A.; Panzella, L.; Crescenzi, O.; Napolitano, A.; Navaratnam, S.; Edge, R.; Land, E. J.; Barone, V.; d'Ischia, M. Lack of visible chromophore development in the pulse radiolysis oxidation of 5,6-dihydroxyindole-2-carboxylic acid oligomers: DFT investigation and implications for eumelanin absorption properties. *J. Org. Chem.* **2009**, *74*, 3727–3734.
- (23) Pezzella, A.; Panzella, L.; Natangelo, A.; Arzillo, M.; Napolitano, A.; d'Ischia, M. 5,6-Dihydroxyindole tetramers with anomalous interunit bonding patterns by oxidative coupling of 5,5',6,6'-tetrahydroxy-2,7'-biindolyl: emerging complexities on the way toward an improved model of eumelanin buildup. *J. Org. Chem.* **2007**, *72*, 9225–9230.
- (24) Arzillo, M.; Pezzella, A.; Crescenzi, O.; Napolitano, A.; Land, E. J.; Barone, V.; d'Ischia, M. Cyclic structural motifs in 5,6-dihydroxyindole polymerization uncovered: biomimetic modular buildup of a unique five-membered macrocycle. *Org. Lett.* **2010**, *12*, 3250–3253.
- (25) Panzella, L.; Pezzella, A.; Napolitano, A.; d'Ischia, M. The first 5,6-dihydroxyindole tetramer by oxidation of 5,5',6,6'-tetrahydroxy-2,4'-biindolyl and an unexpected issue of positional reactivity en route to eumelanin-related polymers. *Org. Lett.* **2007**, *9*, 1411–1414.
- (26) Pezzella, A.; Napolitano, A.; d'Ischia, M.; Prota, G.; Seraglia, R.; Traldi, P. Identification of partially degraded oligomers of 5,6-dihydroxyindole-2-carboxylic acid in Sepia melanin by matrix-assisted laser desorption/ionization mass spectrometry. *Rapid Commun. Mass Spectrom.* **1997**, *11*, 368–372.
- (27) Seraglia, R.; Traldi, P.; Elli, G.; Bertazzo, A.; Costa, C.; Allegri, G. Laser desorption ionization mass spectrometry in the study of natural and synthetic melanins. I-tyrosine melanins. *Biol. Mass Spectrom.* **1993**, *22*, 687–697.
- (28) Reale, S.; Crucianelli, M.; Pezzella, A.; d'Ischia, M.; De Angelis, F. Exploring the frontiers of synthetic eumelanin polymers by high-resolution matrix-assisted laser/desorption ionization mass spectrometry. *J. Mass Spectrom.* **2012**, *47*, 49–53.
- (29) Kroesche, C.; Peter, M. G. Detection of melanochromes by MALDI-TOF mass spectrometry. *Tetrahedron* **1996**, *52*, 3947–3952.
- (30) Tran, M. L.; Powell, B. J.; Meredith, P. Chemical and structural disorder in eumelanins: a possible explanation for broadband absorbance. *Biophys. J.* **2006**, *90*, 743–752.
- (31) Schweitzer Andrew, D.; Howell Robertha, C.; Jiang, Z.; Bryan Ruth, A.; Gerfen, G.; Chen, C.-C.; Mah, D.; Cahill, S.; Casadevall, A.; Dadachova, E. Physico-chemical evaluation of rationally designed melanins as novel nature-inspired radioprotectors. *PLoS One* **2009**, *4*, e7229.
- (32) Edge, R.; d'Ischia, M.; Land, E. J.; Napolitano, A.; Navaratnam, S.; Panzella, L.; Pezzella, A.; Ramsden, C. A.; Riley, P. A. Dopachinone redox exchange with dihydroxyindole and dihydroxyindole carboxylic acid. *Pigm. Cell Res.* **2006**, *19*, 443–450.
- (33) Napolitano, A.; Pezzella, A.; Vincenzi, M. R.; Prota, G. Oxidative-degradation of melanins to pyrrole acids - a model study. *Tetrahedron* **1995**, *51*, 5913–5920.
- (34) Pezzella, A.; Iadonisi, A.; Valerio, S.; Panzella, L.; Napolitano, A.; Adinolfi, M.; d'Ischia, M. Disentangling eumelanin "black chromophore": visible absorption changes as signatures of oxidation state- and aggregation-dependent dynamic interactions in a model water-soluble 5,6-dihydroxyindole polymer. *J. Am. Chem. Soc.* **2009**, *131*, 15270–15275.
- (35) Berne, B. J.; Pecora, R. *Dynamic Light Scattering: with Applications to Chemistry, Biology, and Physics*; Dover Publications: Mineola, NY, 1975; p 400.

(36) Vaccaro, M.; Accardo, A.; Tesauro, D.; Mangiapia, G.; Loef, D.; Schillen, K.; Soederman, O.; Morelli, G.; Paduano, L. Supramolecular aggregates of amphiphilic gadolinium complexes as blood pool MRI/MRA contrast agents: physicochemical characterization. *Langmuir* **2006**, *22*, 6635–6643.

(37) Wignall, G. D.; Bates, F. S. Absolute calibration of small-angle neutron scattering data. *J. Appl. Crystallogr.* **1987**, *20*, 28–40.

(38) Palumbo, A.; D'Ischia, M.; Misuraca, G.; Prota, G. Effect of metal ions on the rearrangement of dopachrome. *Biochim. Biophys. Acta, Gen. Subj.* **1987**, *925*, 203–209.

(39) Mangiapia, G.; Ricciardi, R.; Auriemma, F.; De Rosa, C.; Lo Celso, F.; Triolo, R.; Heenan, R. K.; Radulescu, A.; Tedeschi, A. M.; D'Errico, G.; Paduano, L. Mesoscopic and microscopic investigation on poly(vinyl alcohol) hydrogels in the presence of sodium decylsulfate. *J. Phys. Chem. B* **2007**, *111*, 2166–2173.

(40) Guinier, A.; Fournet, G. *Small-Angle Scattering of X-rays*; Wiley: New York, 1955; p 268.

(41) Ma, G.; Barlow, D. J.; Lawrence, M. J.; Heenan, R. K.; Timmins, P. Small-angle neutron-scattering studies of nonionic surfactant vesicles. *J. Phys. Chem. B* **2000**, *104*, 9081–9085.

(42) Ricciardi, R.; Mangiapia, G.; Lo Celso, F.; Paduano, L.; Triolo, R.; Auriemma, F.; De Rosa, C.; Laupretre, F. Structural organization of poly(vinyl alcohol) hydrogels obtained by freezing and thawing techniques: a SANS study. *Chem. Mater.* **2005**, *17*, 1183–1189.

(43) Roscigno, P.; Paduano, L.; D'Errico, G.; Vitagliano, V. On the presumed specific interaction of anionic surfactants with nonionic polymers. aqueous solution of sodium alkylsulfonate in the presence of poly(vinylpyrrolidone): an “excluded volume” effect. *Langmuir* **2001**, *17*, 4510–4518.

(44) Paduano, L.; Sartorio, R.; Vitagliano, V. Diffusion coefficients of the ternary system α -cyclodextrin–sodium benzenesulfonate–water at 25 °C: the effect of chemical equilibrium and complex formation on the diffusion coefficients of a ternary system. *J. Phys. Chem. B* **1998**, *102*, 5023–5028.

(45) Annunziata, O. Private communication, 2008.

(46) Molisso, A. *Idrogeli modificati di PVA: Studio del comportamento di fase del PVA in presenza di sali semplici e polimeri*; Università degli Studi di Napoli “Federico II”: Naples, 2008.

(47) Gallas, J. M.; Zajac, G. W.; Sarna, T.; Stotter, P. L. Structural differences in unbleached and mildly-bleached synthetic tyrosine-derived melanins identified by scanning probe microscopies. *Pigm. Cell Res.* **2000**, *13*, 99–108.

(48) Napolitano, A.; Pezzella, A.; Prota, G.; Seraglia, R.; Traldi, P. Structural analysis of synthetic melanins from 5,6-dihydroxyindole by matrix-assisted laser desorption/ionization mass spectrometry. *Rapid Commun. Mass Spectrom.* **1996**, *10*, 468–472.

(49) Marks, M. S.; Seabra, M. C. The melanosome: membrane dynamics in black and white. *Nat. Rev. Mol. Cell Biol.* **2001**, *2*, 738–748.

(50) Clancy, C. M. R.; Nofsinger, J. B.; Hanks, R. K.; Simon, J. D. A hierarchical self-assembly of eumelanin. *J. Phys. Chem. B* **2000**, *104*, 7871–7873.